Influence of metal ions on thermo-oxidative stability and combustion response of polyamide 6/clay nanocomposites

Zope, Indraneel Suhas; Dasari, Aravind; Guan, Fanglan; Yu, Zhong-Zhen

2016

Zope, I. S., Dasari, A., Guan, F., & Yu, Z.-Z. (2016). Influence of metal ions on thermo-oxidative stability and combustion response of polyamide 6/clay nanocomposites. Polymer, 92, 102-113.

https://hdl.handle.net/10356/83309

https://doi.org/10.1016/j.polymer.2016.03.087

Influence of metal ions on thermo-oxidative stability and combustion response of polyamide 6/clay nanocomposites.

Indraneel S Zope[a], Aravind Dasari[a,*], Fanglan Guan[b], Zhong-Zhen Yu[b]

[a]School of Materials Science & Engineering (Blk N4.1), Nanyang Technological University, 50 Nanyang Avenue, Singapore 639798

[b]State Key Laboratory of Organic-Inorganic Composites, College of Materials Science and Engineering, Beijing University of Chemical Technology, Beijing 100029, China

ABSTRACT:

Combustion and thermo-oxidative properties of polyamide 6 (PA6)/montmorillonite (MMT) clay nanocomposites are studied with emphasis on the catalytic role of metal ions (Mg^{2+}, Al^{3+} and Fe^{3+}) present in MMT. Each metal ion uniquely influences condensed phase reactions (mechanism and/or kinetics) depending on its concentration in metal ion exchanged MMT, its ability to form metal-organic complexes, and confinement effect as determined by eventual dispersion of MMT in the matrix. Presence of Al^{3+} accelerated kinetics of PA6 decomposition during initial stages, Mg^{2+} rich composite displayed good thermo-oxidation stability and char yield, and Fe^{3+} prominently altered the chemical composition of condensed phase ultimately producing highest amount of smoke. Possible PA6 decomposition reaction mechanisms have been identified that are susceptible to metal ion catalysis in the presence of oxygen. These results provide important progress towards the understanding of widely reported yet poorly understood phenomena of catalyzing effect of clay during the combustion of polymer. The results are a

definite step towards the realization of stand-alone clay based nanocomposites with superior fire retardancy.

KEYWORDS: *catalysis, thermo-oxidation, combustion, polyamide 6, montmorillonite, mechanism*

*Corresponding author:

E-mail: aravind@ntu.edu.sg; Fax: +65-6790 9081

1. Introduction

During combustion, polymer/clay nanocomposites show low heat release rates (HRR) even at reduced clay loading levels. However, poor ignition resistance is restricting their potential as a standalone flame retardant [1,2]. Though a number of physio-chemical theories have been proposed to elucidate their ignition characteristics [3-13], there still remain a missing mechanistic link that can decisively associate early ignition to a structural aspect of clays. Clay activated catalyzation demonstrated by Fina et al. [13] emphasized the chemical reactivity of clays lead to critical fuel concentration quickly with lower thickness of surface material contributing to fuel production. Another important contribution to this facet came from Carvalho et al. [14]. They provided preliminary experimental evidence of, otherwise widely theorized, radical trapping effect by Fe^{3+} from clay and its influence on polymer decomposition. This highlighted the fact that clay layers can alter combustion chemistry of polymer/clay nanocomposites in addition to the well-known physical barrier effect. However, there are various structural aspects of clay that are needed to be considered to understand source and nature of a

catalytic site. Some of them include: acidity of surface hydroxyl groups, number of defect sites and edges exposing unbalanced structural metal ions, type of exchange cations, and dehydration along with dehydroxylation temperatures.

Metal ions' interaction with PA6 is rather complex. Some metal ions like Fe^{3+}, Cu^{2+} and Zn^{2+} coordinate directly with carbonyl oxygen from amide link (direct coordination); while Mg^{2+} and Ca^{2+} coordinate with compounds facilitating their hydrogen bonding with carbonyl oxygen from amide linkages (indirect coordination) as represented in Fig. 1A [15-17]. Metal-amide complexes may in turn alter crystal structure of PA6 by hindering hydrogen bonding [18]. Complexes with certain metal ions (like Cu^{2+} and Zn^{2+}) increase the electrophilic nature of carbonyl carbon towards (amide) hydrolysis even under neutral conditions [19]. The reported tautomeric structures for metal-amide complex (Fig. 1B) [20] could influence β-hydrogen abstraction. Further, metal ions can also coordinate with carbonyl compounds with amide/imide linkages like oxamide [21] or ε-caprolactam [22]. Fig. 2 indicates intermediate (carbonyl) decomposition products commonly generated during PA6 thermo-oxidation that can potentially coordinate with metal ions on clay surface. Strength and degree of this coordination depend on factors like spatial restriction for reorientation of ligand molecule/segment, position of coordinating segments (i.e. along chain length or at terminal ends), electronegativity of metal ion, and conjugation.

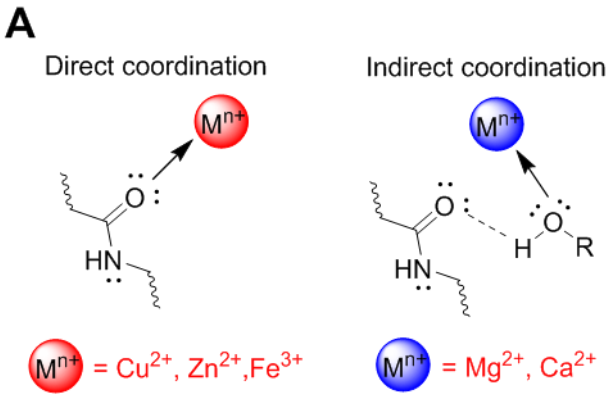

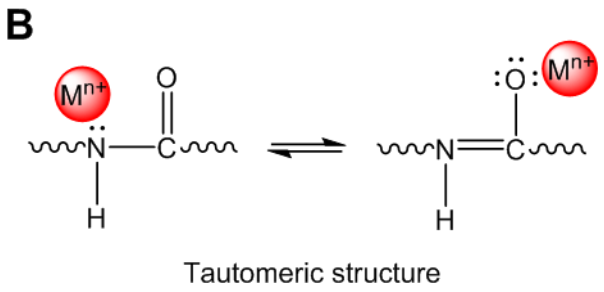

Fig. 1. (A) Structure of PA6-metallo complex depending on metal ion [15-17] (B) Tautomer for metal ion-amide linkage [20]. (Single column fitting image)

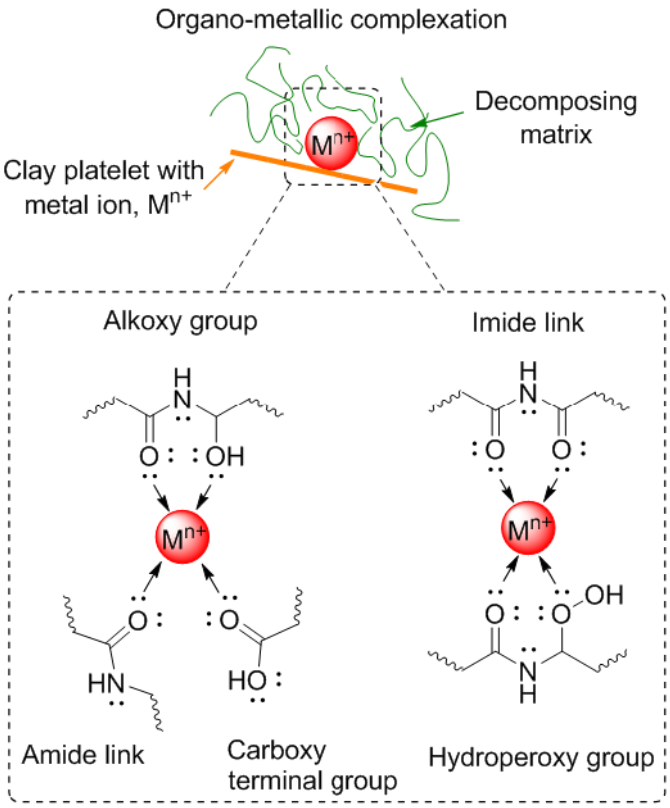

Fig. 2. Potential coordination complexes at organo-clay interface between metal ion and carbonyl compounds generated during PA6 thermo-oxidation. (Single column fitting image)

It is widely accepted that PA6 follows peroxy-based decomposition mechanism under thermo-oxidative conditions generating reactive alkoxy- and peroxy- moieties during initial stages of decomposition. Metal ions can accelerate the generation of these intermediate reactive moieties, and also influence oxidative stability of the char (depending on their redox potential, concentration and chelation) [19,23-25]. We found this to be valid as significantly varying effects for different metal ion exchanged clays, depending on principle metal ion (Mg^{2+}, Al^{3+} or Fe^{3+}), were observed on decomposition onset of organic modifier and oxidative stability of carbonaceous matter [26]. Each metal ion enriched clay exhibited unique Brønsted acidity and Lewis acidity, which subsequently altered decomposition mechanism of organic modifier. In the following work, we incorporated these metal ion (Mg^{2+}, Al^{3+} and Fe^{3+}) enriched clays in PA6 to investigate their effect on different decomposition stages of PA6 under thermo-oxidative conditions.

2. Experimental

2.1 Materials and synthesis procedure

Ultramid B3S (trade name of PA6) was supplied by BASF, Singapore. It has a melting point of 220 ^{o}C and a V-2 rating in UL94 (vertical burning test) at 1.6 mm thickness. Prior to melt compounding, PA6 was dried at 90 ^{o}C for 24 hours in a convection oven. Sodium MMT, commercially known as Cloisite Na^{+}, was procured from BYK-Chemie GmbH. Cloisite Na^{+} has a mean formula unit of $Na_{0.65}[Al,Fe]_4Si_8O_{20}(OH)_2$ and cation exchange capacity, CEC, of 92 meq/100 g. Preparation of metal ion exchange clays (MI-clays) and organically modified MI-clays (OMI-clays) using hexadecyltrimethylammonium ion is reported earlier [26].

Melt mixing of 5 wt.% clay with PA6 was carried out using Leistritz Micro 18 twin screw extruder at 80 rpm. The granulated material was compression molded into test specimens (100 mm x 100 mm x 5 mm) for cone calorimeter testing using Carver Hot Press maintained at 250 ^{o}C with molding pressure of 5 bar and total molding time of 20 min.

2.2 Characterization

X-ray diffraction (XRD) measurements of molded samples along with finely granulated residues were performed on Shimadzhu XRD 6000 (40 kV, 30 mA, Cu kα, λ = 1.542 Å) with a scan speed of 1 ^{o}/min, scan range of 3-45^{o} and step size of 0.02^{o}. Melting and crystallization characteristics of neat PA6 and its composites were determined using a differential scanning calorimeter, DSC, from TA Instruments (model: Q10). Two complete heating/cooling cycles between 30 - 240 ^{o}C were performed at a rate of 10 ^{o}C/min. Fourier transform infrared (FTIR) spectra of PA6 materials, clay and powdered residues (prepared using KBr pellets) were collected using Perkin-Elmer SpectrumGX spectrometer and Perkin-Elmer Frontier Spectrometer (surface ATR FTIR). All spectra were acquired in the range of 400-4000 cm^{-1} using 64 scans and resolution of 1 cm^{-1}. To observe clay dispersion in polymer matrix, trimmed polymer composite samples were ultra-microtomed at 0.2 mm/s using a diamond knife on Leica Ultracut UCT in liquid N_2 environment at –100 ^{o}C to get 70-90 nm thick sections. The sections were picked up using a droplet of 2.3 mol sucrose and placed on formvar/carbon coated 400-mesh copper grids. After thorough rinsing with distilled water to wash away the sucrose, sections were observed using a Carl Zeiss transmission electron microscopy (TEM), LIBRA 120, in bright field mode and at an accelerating voltage of 100 kV.

2.3 Thermal and combustion tests

To understand the decomposition products, thermogravimetric analyzer coupled with FTIR (TG-IR) was used. This system is from Perkin-Elmer TGA-7 with TGA Pyris 7.0 software having an interface with Perkin-Elmer Spectrum GX system for FTIR. Temperature range employed was from 30 ^{o}C to 750 ^{o}C at a heating rate of 20 ^{o}C/min. Dry air at a flow rate of 20 mL/min carried decomposition gaseous products through IR interface into IR detection chamber. To prevent any condensation, metal transfer line as well as FTIR gas cell was maintained at 150 ^{o}C. All IR spectra were acquired in the range of 400-4000 cm^{-1} using one scan with a resolution of 2 cm^{-1}. Consecutive readings were taken with a time interval of ~11.3 sec (i.e., 3.7 ^{o}C resolution). Cone calorimeter from Fire Testing Technology was used to determine the combustion response of compression molded PA6 and its composites. The tests were carried out according to ISO 5660 at an irradiant heat flux of 35 kW/m^2. Isothermal studies were carried out using Nabertherm muffle furnace Model LE4/11 preheated to desired temperature with 30 min temperature stabilization time. For isothermal studies, 5 g of material was placed in furnace for 5 min preheated at 325, 350, 375, 400, 425, 450 and 475 ^{o}C, while 20 g of material and 15 min were used when the temperature of operation was 750 ^{o}C.

3. Results and discussions

3.1 Crystal phase and microstructure

It is known that polyamides seek to maximize the number of H-bonds within and between polymer chains. This process requires polyamide chains to adopt either a fully extended or a twisted configuration determining the resulting crystal form, monoclinic α- or pseudo-hexagonal γ-phase. However, with the incorporation of MMT platelets, many studies have reported that a γ-

phase is favored instead of α-form (see for instance, ref [27]). This was believed to be a result of chain conformation change (pointing to the extent of dispersion of clay layers in the matrix), limiting the formation of H-bonded sheets of polyamides. In line with this, even in the current work, strong γ phase peaks (10.7^o and 21.3^o) for PA6/OMI-clay composites are observed suggesting good dispersion of OMI-clay in PA6 matrix. Diffraction patterns for all composites are provided in Supporting Information (Fig. S1). TEM micrographs shown in Fig. 3 further confirm this. PA6/MI-clay composites, however, displayed prominent diffraction peaks corresponding to α phase (20.5^o and 24^o) indicating limited dispersion of MI-clays in PA6. To further corroborate these results, DSC tests are carried out and the results are shown in Supporting Information as Fig. S2. In addition to melting peak at 221 ^{o}C corresponding to α phase, only OMI-clay composites displayed a lower melting γ phase peak at 210 ^{o}C.

Nonetheless, the prominence of α or γ might not be a direct indicator of dispersion. Li et al. [28] showed that the addition of fibrillar multi-walled carbon nanotubes to polyamide favor α-phase instead of γ (even with well dispersed nanotubes). However, they also observed that with amino-functionalization of multi-walled carbon nanotubes, γ-form was preferred over α. This shows that stronger interaction between fillers and PA6 could force PA6 chains out of hydrogen-bonded sheets of the α-form and promote crystallization in the γ-form. Similarly, the effect of metal cations on this process was also discussed in a few studies, which showed that amide-metal complexation is a major parameter influencing hydrogen bonding and thereby, crystallinity (and melting point). More discussions on this aspect are provided in the Supporting Information section.

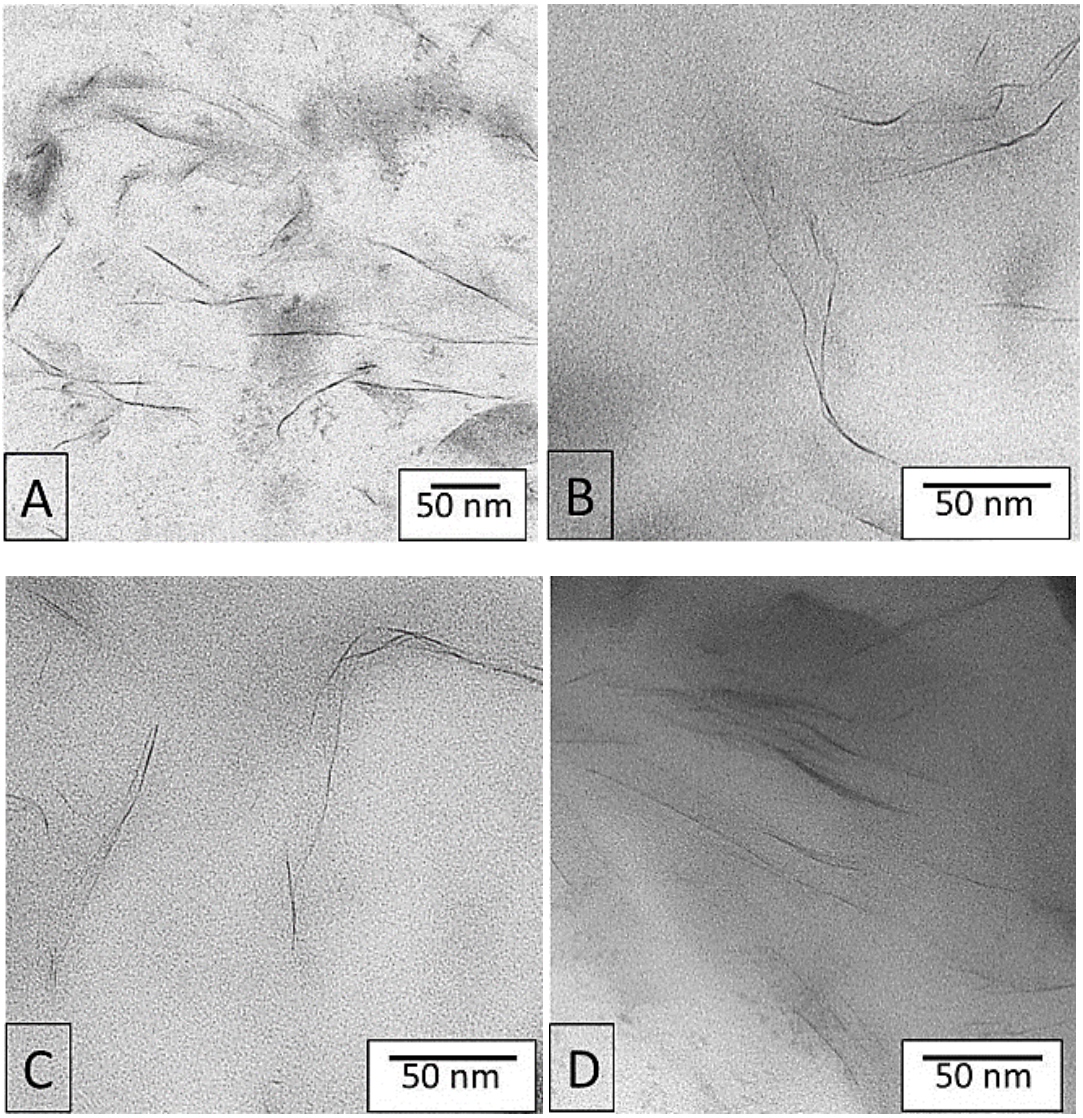

Fig. 3. Representative TEM images of PA6/OMI-clay nanocomposites; (A) PA6/ONaMMT, (B) PA6/OMgMMT, (C) PA6/OAlMMT, and (D) PA6/OFeMMT. (Single column fitting image)

3.2 Combustion properties

Combustion properties of neat PA6 and its composites obtained from cone calorimeter are listed in Table 1. With OMI-clays, TTI values of nanocomposites improved (over PA6/MI-clay composites) and this is attributable to lower concentrations of residual exchangeable metal ions on OMI-clay surfaces, as discussed and confirmed in our earlier study [26]. Better dispersion of

clay platelets in PA6/OMI-clay nanocomposites compared to PA6/MI-clay composites is another factor that can affect TTI values. Among all the samples, PA6/AlMMT composite displayed quickest ignition time of 83 s. Even with OAlMMT, TTI value is still 92 s suggesting the dominance of catalytic effect of Al^{3+}. Similar (catalytic) activity was also reported in polypropylene samples filled with Al-POSS where TTI was reduced by 19 s compared to neat polypropylene [29]. In short, comparing TTI values of all samples, it is clear that pre-ignition reactions depend on combined effects of type/nature of metal ions on clay particles and the physical barrier (more detailed discussions on these aspects in later sections).

Table 1. Cone calorimeter results of neat PA6 and its composites with MI-clays and OMI-clays.

(Double column fitting table)

Specimen	TTI (s)	pHRR (kW/m²)	Avg. HRR (kW/m²)	THR (MJ/m²)	Char (%)	TSR (m²/m²)	TSP (m²)
PA6	140	840	298	97	0	108	0.96
PA6/NaMMT	94	826	349	148	12.4	427	3.77
PA6/MgMMT	85	535	261	113	34.2	586	5.18
PA6/AlMMT	83	566	263	113	28.5	425	3.76
PA6/FeMMT	100	543	295	147	17.6	737	6.52
PA6/ONaMMT	116	369	257	147	11.9	1133	10.02
PA6/OMgMMT	114	327	229	151	10.0	1087	9.61
PA6/OAlMMT	92	368	254	154	10.6	1035	9.15
PA6/OFeMMT	107	397	253	161	6.2	1354	11.97

TTI: time to ignition; pHRR: peak values of HRR; THR: total heat released; TSR: total smoke released; TSP: total smoke produced

Beyond TTI, the influence of principle metal ion (Na^{+}, Mg^{2+}, Al^{3+} or Fe^{3+}) is also evident on HRR, % char, and smoke parameters (TSP and TSR). Peak HRR values, as expected, show a dependence on dispersion of clay platelets in the matrix; relative reductions of up to 36% in peak HRR values are obtained with PA6/MI-clay samples and up to 61% with PA6/OMI-clay nanocomposites compared to neat PA6 (Fig. 4). Further, PA6/MgMMT composite gave highest char of ~34 % followed by PA6/AlMMT with ~28 % and PA6/FeMMT with ~17 %. These results are also in line with our previous work where it was found that Mg^{2+} and Al^{3+} delayed the oxidation of carbonaceous matter, whereas Fe^{3+} catalyzed the oxidation process [26]. Similar trend is seen with PA6/OMI-clay nanocomposites. These values of % char clearly point to enhanced crosslinking as a result of complex formation [30]. Even in a recent study, it was reported that when Ba^{2+} (alkaline earth metal like Mg^{2+}) was incorporated into sodium alginate fibers, a high char value of 34.2 % was obtained (in TGA under air atmosphere until 900^{o}C) [31]. Without the divalent cation, only 0.63 % char was obtained.

PA6/FeMMT composite, despite showing similar reduction in peak HRR value as PA6/MgMMT and PA6/AlMMT composites, its total heat release (THR), TSR and TSP values are higher. Similar trend is seen with PA6/OFeMMT sample as well. Moreover, with same THR value as PA6/AlMMT, PA6/MgMMT produced ~6 % more char and also registered ~28 % higher TSR and TSP. This again indicates that these cations are playing an active and unique role in PA6 decomposition process, possibly, altering decomposition kinetics and/or mechanism. In one of the early studies on metal-catalyzed polymer oxidation [22], it was reported that addition 0.5 wt.% of metal stearate to polypropylene (PP), which also follows peroxy-based thermo-oxidation similar to PA6, resulted in different oxygen uptake rates in the order of Fe^{3+}>Al^{3+}>Mg^{2+}>control PP. Activation energy for auto-oxidation was also lower for metal-

containing PP by ~25 kJ/mol than neat PP. It was hypothesized that there may be a correlation between catalytic activity of metal salt and decomposition of hydroperoxide.

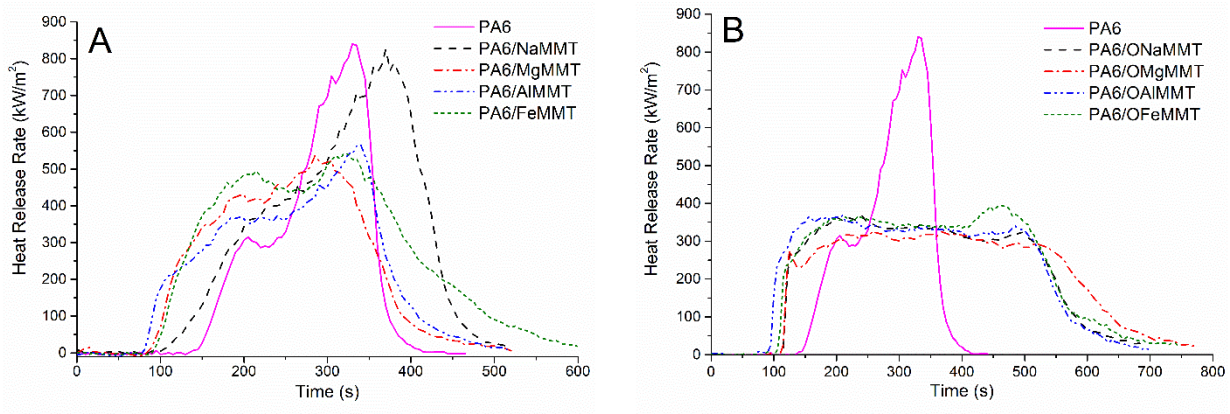

Fig. 4. HRR curves of PA6 and its composites with (A) MI-clays, (B) OMI-clays. (Double column fitting image)

3.3 Thermo-oxidative degradation behavior of PA6 nanocomposites

Onset temperature at 5 % mass loss ($T_{5\%}$), temperature at 50 % mass loss ($T_{50\%}$) and peak temperature for degradation step (T_P) as obtained from TGA under oxidative conditions are summarized in Table 2 and the TGA curves are shown in Fig. 5. Interestingly, Al-rich composites showed the lowest $T_{5\%}$ in their respective group similar to TTI values, confirming its catalytic reactivity towards PA6 matrix. Beyond this, $T_{5\%}$ values of other PA6/MI-clay and PA6/OMI-clay nanocomposites are similar. For PA6/MI-clay composites, $T_{50\%}$ and T_P are similar to that of neat PA6, but in the presence of organically modified clays, the values are slightly higher. For example, in the case of OMgMMT composite, there is ~30 ^oC increment in T_P and ~19 ^oC in $T_{50\%}$. This is despite clear differences in mass loss rate profiles of MI-clay composites (in particular) compared to neat PA6. This suggests a similarity in kinetics and

probable dissimilarity in mechanisms in PA6/MI-clay composites; and vice-versa in PA6/OMI-clay nanocomposites (similar mechanisms but dissimilar kinetics).

Based on the thermo-oxidative degradation data of MI-clays and OMI-clays[26], we believe that these results are a consequence of combined effects of Lewis acidity, clay dispersion and confinement. In PA6/MI-clay composites, polyamide chains that are *confined* in the interlayers of clay platelets will have a higher probability of exposure to metal ions (see Fig. S3 in Supporting Information). This either affects the stability of intermediate decomposition products or results in the formation of different decomposition products. In PA6/OMI-clay nanocomposites, the degree of confinement of polymer chains within the intra-gallery is less. Though the concentration of metal ions on clay platelets is less, exfoliated morphology could provide an opportunity for enhanced interaction throughout the volume. Depending on the inherent (catalytic) nature of metal ions, it is believed that uniform generation of peroxy and hydroperoxy radical moieties in the condensed phase (of PA6 with OMI-clays) would enhance the recombination reactions. This results in delay of peak decomposition temperatures (i.e., altered decomposition kinetics). Further, lack of stearic hindrance near the clay surface provides favorable conditions for surface metal ions to form coordinate complexes with near-by peptide linkages or carbonyl groups. This in turn affects metal ions reactivity similar to inhibitory action of certain chelating agents. For example, Osawa [22] observed that the oxidizing effect of Cu^{2+} was reduced as a result of its coordination with oxamide and its derivatives. Moreover, stable coordination and prolonged proximity of (intermediate decomposition) compounds around clay surface might result in localized crosslinking, *shielding* the clay surface.

Another important observation is the small mass loss peak around 565 ^{o}C for PA6/NaMMT and PA6 composites with FeMMT and OFeMMT due to the catalytic-oxidation effect of Fe^{3+} on

carbonaceous residue. This in fact supports the argument justifying lower % char for PA6/FeMMT and PA6/OFeMMT composites. To verify this and other arguments discussed earlier, condensed phase analysis using FTIR and XRD, and gas phase analysis using FTIR are carried out and discussed below.

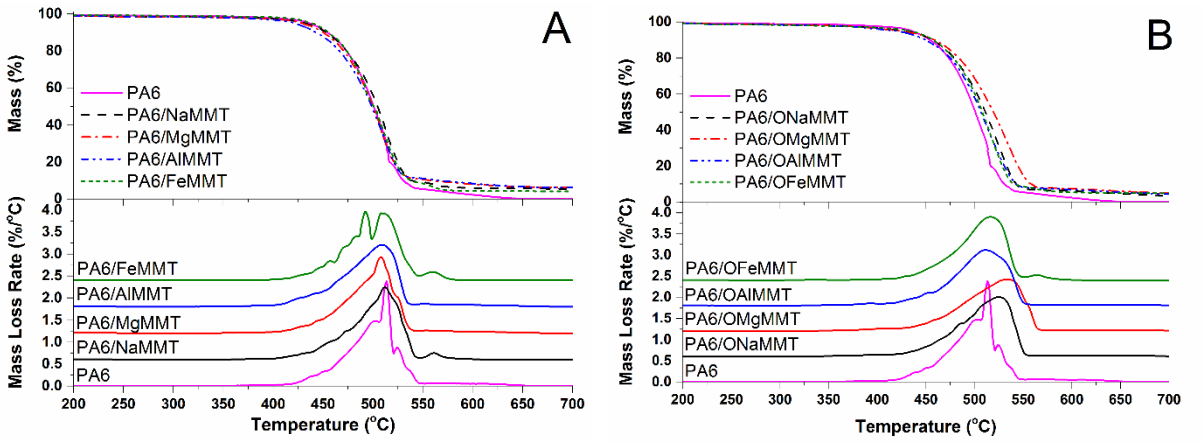

Fig. 5. TGA thermograms of PA6 and its composites with (A) MI-clays, and (B) OMI-clays.

(Double column fitting image)

Table 2. $T_{5\%}$, $T_{50\%}$ and T_P as obtained from TGA thermograms for PA6 and its composites.

(Single column fitting table)

Specimen	$T_{5\%}$ (°C)	$T_{50\%}$ (°C)	T_P (°C)
PA6	437	501	504
PA6/NaMMT	432	505	513
PA6/MgMMT	429	500	508
PA6/AlMMT	422	499	508
PA6/FeMMT	439	501	511
PA6/ONaMMT	430	511	525
PA6/OMgMMT	425	520	534

PA6/OAlMMT	421	507	511
PA6/OFeMMT	434	508	516

3.4 Condensed phase analysis

3.4.1 Isothermal heating between 325-475 ^{o}C

To understand the early stages of degradation of PA6 and development of char, all samples are isothermally heated for 5 min in the temperature regime of 325-475 ^{o}C with a 25 ^{o}C step and ATR FTIR spectra is taken from the surface of residues. Only the spectra corresponding to neat PA6, PA6/FeMMT and PA6/OFeMMT samples are shown in Figs. 6 and 7 as representative of the phenomenon and curves for other samples are presented as Fig. S4 in Supplementary Information due to similarity. Fig. 6 reveals the following spectral features for neat PA6:

1. shoulder peaks, though weak, at 1712 cm^{-1} and 1762 cm^{-1} point to the formation of carbonyl moieties (aldehydic, ketonic or carboxylic carbonyl); and
2. isocyanate peak between 350-400 ^{o}C, but it is unclear if this peak continues to exist beyond 400 ^{o}C as it is overlapped by stronger nitrile group peak from 425 ^{o}C.

In PA6 composites, apart from the above, the evolution of nitrile moieties with temperature is dependent on the type of metal ion (Figs. 7 and 8). Except Mg^{2+}, all other composites show a drop in intensity with increase in temperature (up to 475 ^{o}C). Fe^{3+} containing composite shows a peak at 400 ^{o}C, while with Al^{3+}, peak is at 450 ^{o}C similar to neat PA6. This highlights the relative concentration (qualitative) of nitrile moieties. The results reiterate the significant influence of metal ions on kinetics and/or mechanism. Differences between PA6/FeMMT or OFeMMT and neat PA6 in the temperature regime studied are also highlighted in Table 3 for simple viewing.

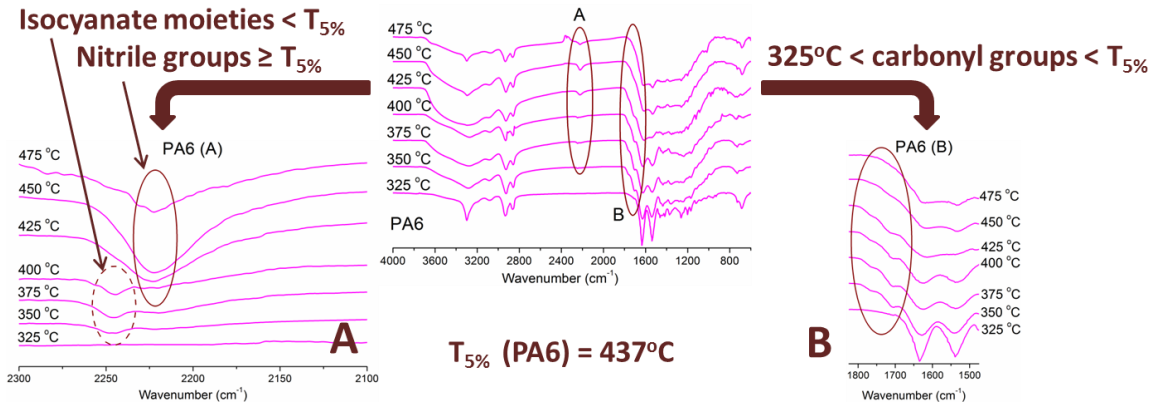

Fig. 6. Overlay of FTIR spectra for isothermally heated PA6 between 325 and 475 °C. (Double column fitting image)

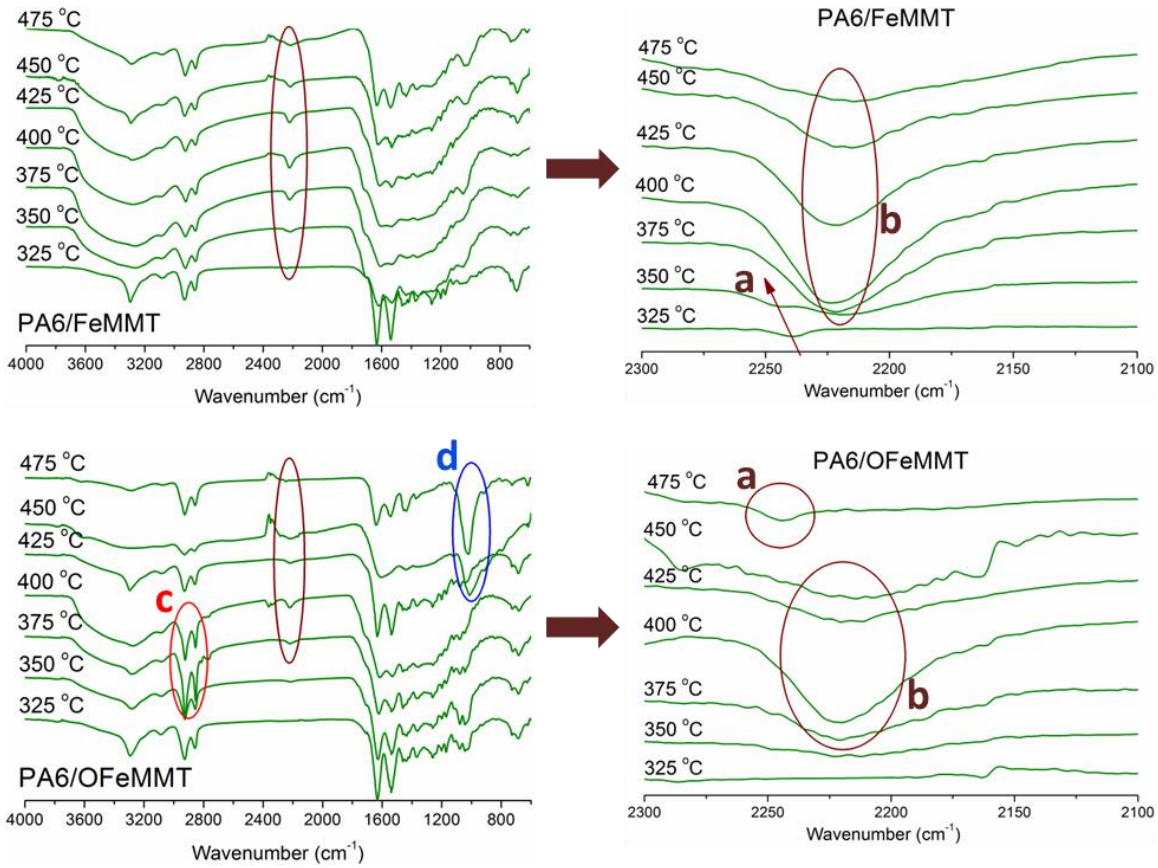

Fig. 7. Overlay of FTIR spectra for isothermally heated PA6/FeMMT and PA6/OFeMMT composite. Isocyanate peak (indicated by 'a') shifted by 12 cm^{-1} between 325 and 350 ^{o}C for PA6/FeMMT, while PA6/OFeMMT display isocyanate peak even at 475 ^{o}C; both PA6/FeMMT and PA6/OFeMMT display nitrile peak (indicated by 'b') below their respective $T_{5\%}$ (439 ^{o}C and 434 ^{o}C); PA6/OFeMMT display strong aliphatic carbon peak at 375 ^{o}C indicated by 'c' and development of strong Si-O peak from 450 ^{o}C ('d') that is below its $T_{50\%}$ (508 ^{o}C). (Double column fitting image)

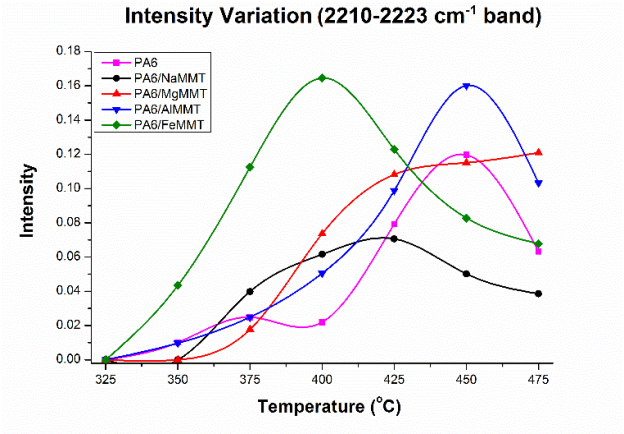

Fig. 8. Variation in peak intensities corresponding to nitrile group for PA6 and PA6/MI-clay composites between 325 and 475 ^{o}C. Intensity was measured using temporary base line in the range of 2300-2100 cm^{-1}. (Single column fitting image)

Table 3. IR bands observed as a result of isothermal heating of PA6 and its Fe-based composites. (Double column fitting table)

Absorption range, cm^{-1}	Assignments	Analysis
2950-2830	$–CH_3$, $–CH_2–$ aliphatic	Only PA6/FeMMT display these strong bands in the range of 2950-2830 cm^{-1} and only between 350 and 400 ^{o}C suggesting

	carbon, stretch	accelerated generation of aliphatic carbon moieties in condensed phase.
2250-2240	N=C=O in isocyanate, anti-sym. stretch	Isocyanate peaks for PA6/FeMMT remain inconclusive due to possible overlapping with broad nitrile peak. However, a distinct weak isocyanate peak for PA/OFeMMT is seen at 475 ^{o}C due to absence of nitrile peak at that temperature, hence it is suggested that isocyanate moieties are stable even at 475 ^{o}C.
2230-2210	C=N in nitrile, stretch	Strength of nitrile peaks in both PA6/FeMMT and PA6/OFeMMT is stronger even at temperatures of 375 ^{o}C.
1606-1775	C=O in carbonyl moieties, stretch	After deconvolution of the spectra obtained at 375 ^{o}C in the range of 1900-1550 cm^{-1}, it is clear that PA6/FeMMT shows a shift of ~22 cm^{-1} from 1628 to 1606 cm^{-1} indicating back-bonding of Fe^{3+}-amide linkage complex (Fig. 9). Similarly, shifts of ~11 and 13 cm^{-1} are also observed in the carbonyl peaks to higher wavenumbers 1723 and 1775 cm^{-1}. This might be due to the generation of different carbonyl moieties than those formed in neat PA6. In PA6/OFeMMT nanocomposite, there is no presence of any peak corresponding to C=O above 1760 cm^{-1}.
1150-1050	Si–O–Si in MMT, stretch	This peak appears for PA6/OFeMMT at temperatures as low as 450 ^{o}C before $T_{50\%}$ (508 ^{o}C) is reached. This confirms that clay migration for exfoliated morphologies start at temperatures lower than those for intercalated morphologies [32] (like PA6/FeMMT).

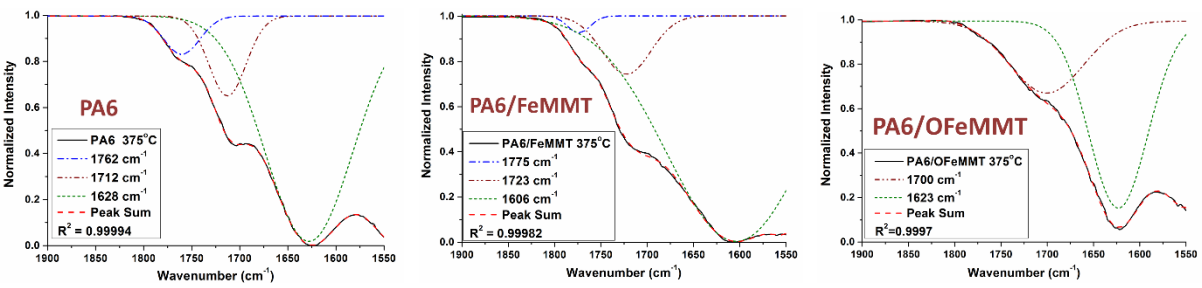

Fig. 9. Deconvoluted FTIR ATR spectra in the range of 1900-1550 cm^{-1} from the surface of residues of PA6 and its Fe-based composites after isothermal heating at 375 ^{o}C. (Double column fitting image)

3.4.2 Isothermal heating at 750 ^{o}C

Two major (interlinked) differences in FTIR and XRD data of PA6/MI-clay and PA6/OMI-clay composites are evident in Fig. 10: (i) $–CH_3$ and $–CH_2–$ (stretching) peaks in FTIR at ~2925 and 2850 cm^{-1} and (ii) intensity and breadth in x-ray diffraction peaks in the 6 - 9^{o} range and at 27.5^{o}. These highlight compositional concentration changes of carbonaceous residue entrapped between collapsed clay platelets. For instance, peak between 6 - 9^{o} is a direct indication of oxidizing capacity of each cation during late stages of charring. As we have reported earlier [26], Fe^{3+} enhances oxidation of carbonaceous matter explaining the significantly less intense peak at 7^{o} for both PA6/FeMMT and PA6/OFeMMT residues. The nature of this carbonaceous matter is represented by the peak at 27.5^{o}, which is generally ascribed to (002) plane in graphitic structure and is consistently observed in polymer/clay nanocomposite residues [30]. More importantly, PA6/OMI-clay residues do not show expected reduction in peak intensities associated with –OH stretching (~3640, ~3410 cm^{-1}) and –OH bending vibrations (~1645 cm^{-1}) that are linked to dehydroxylation of clay. This signifies the presence of surface and/or coordinated water even at 750 ^{o}C, which is generally not expected. This points to the clay shielding effect described earlier. That is, depending on the interaction and inherent catalytic activity of cation, PA6 can decompose preferentially around the clay platelet generating a coat of carbonaceous residue. This shield could delay clay dehydroxylation

and prohibit the interaction of interlayer cations with neighbouring organic matter. Some other minor differences among the samples suggesting metal ion migration in MMT are explained in the Supporting Information section (Fig. S5).

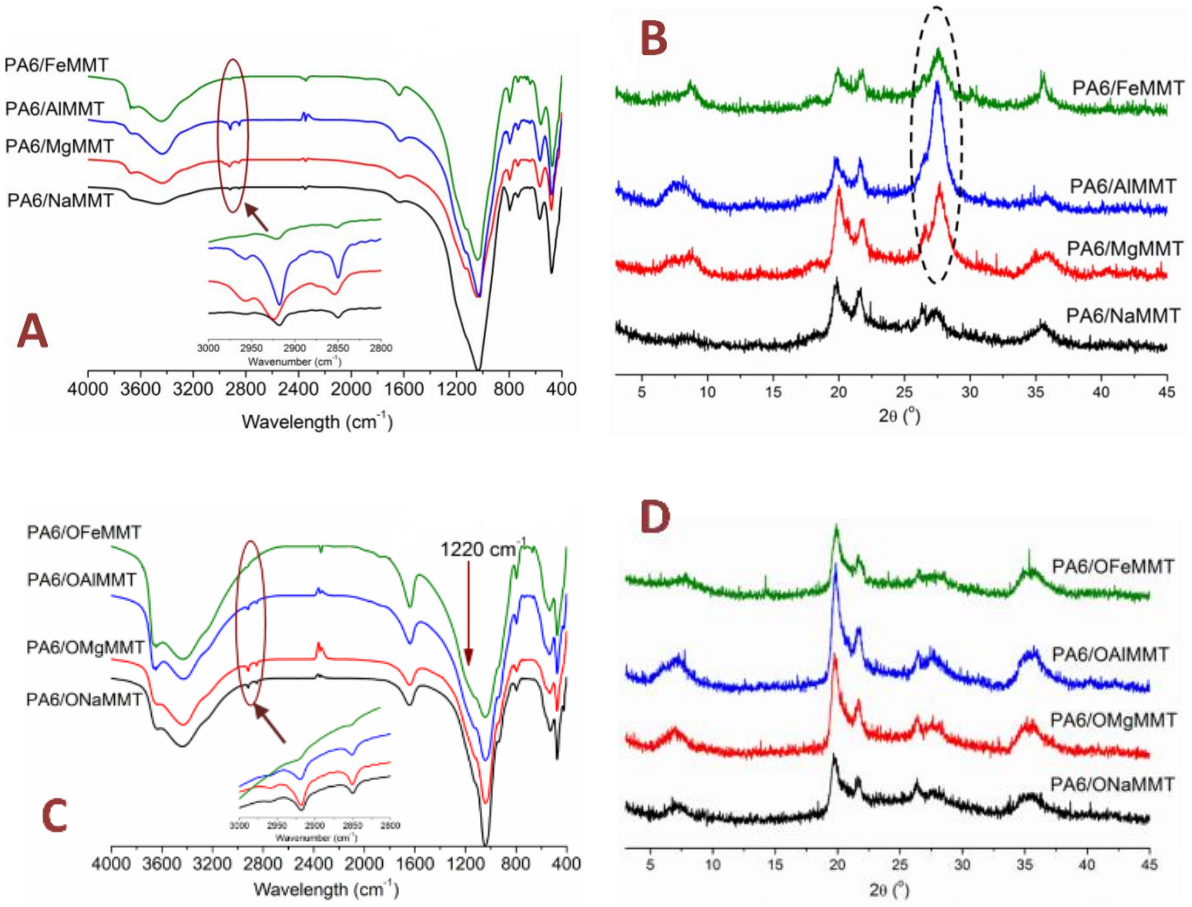

Fig. 10. (A) FTIR spectra and (B) XRD curves of PA6/MI-clay composites. (Double column fitting image)

3.5 Gas phase analysis using TG-IR

A four-stage evolution process for CO_2 is seen from the 3D TG-IR plot of neat PA6, Fig. 11, inset A. By correlating this data with TGA results discussed earlier, it is evident that the first stage corresponds to $T_{5\%}$, second and third stages to oxidation of decomposition products, while

the final stage is a result of oxidation of char. Inset B highlights absorbance signals of evolved products. Apart from the peaks corresponding to CO, CO_2, H_2O and primary amines, strong signals at ~1640 and 2890 cm^{-1} corresponding to cyclo-ketones (cyclopentanone and cyclohexanone) and ε-caprolactam, respectively, are observed. This assignment is made considering gas chromatography coupled with mass spectroscopy results of Michal et al. [33]. They reported that cyclopentanone and cyclohexanone constitute ~46 % of total evolved gases for PA6 under thermo-oxidative conditions. Expectedly, only 1.2 % was registered to ε-caprolactam. However, array of peaks seen in Fig. 11 in the range of 1730-1760 cm^{-1} also suggest formation of other carbonyl groups like aldehyde or carboxylic acid.

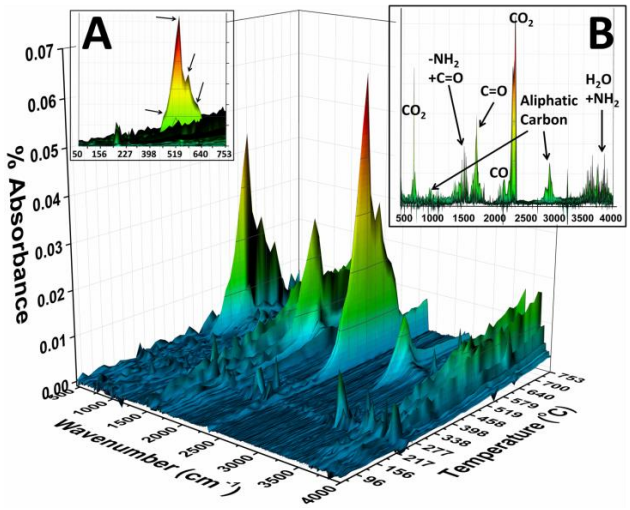

Fig. 11. TG-IR spectrum of PA6. The arrows in inset A indicate the steps corresponding to evolution of CO_2. (Single column fitting image)

Comparing TG-IR data of PA6 with PA6/MI-clays (Figs. 11-12), differences are apparent in (i) 3000-4000 cm^{-1} region, in which, traditionally, peaks are associated with –OH, –NH and CO_2; and (ii) around 2350 cm^{-1} (CO_2 evolution profile). Peak intensity in the 3000-4000 cm^{-1} range

successively reduced for MI-clay composites in the order of Na^{+}>Mg^{2+}>Al^{3+}>Fe^{3+}. Interestingly, this reduction overlaps with increase in Lewis acid character from Na^{+} to Fe^{3+}. This again suggests greater coordination character. As a result, intermediate decomposition products like acrylamide imide attain certain stability that are otherwise prone to thermal dissociation without accumulation in PA6 [34]. This obviously influences decomposition kinetics. The presence of confined environment within the intercalated PA6/MI-clay composites, might as well provide favorable conditions for enhancing the interfacial interaction between metal ions on clay surface and constrained matrix/intermediate decomposition products. It has also been reported that these confined conditions resulted in same product with different conformation, which otherwise, was not energetically favorable [35].

Absence of profound differences between PA6 and PA6/NaMMT (Figs. 11 and 12A) in 3000-4000 cm^{-1} range, suggest that Na^{+} does not significantly alter the decomposition mechanism of PA6, which highlights restricted capability of Na^{+} (on clay surface) to form coordination complexes [36]. However, Na^{+} influence oxidation stability of carbonaceous matter giving additional CO_2 peak at 570 ^{o}C, similar to Fe^{3+}, and stronger than the one observed in neat PA6. It was observed that oxidation of PA6 at 400 ^{o}C in the presence of 'Na-salts' gave 70 % less HCN and 15-35 % more ammonia [37]. This was attributed to the reaction of sodium ions with HCN inhibiting HCN evolution by forming NaCN. However, no such evidence of NaCN formation was provided raising questions on the hypothesis put forth. Even in the current work, there is no indication of NaCN presence in the condensed phase. For PA6/AlMMT, a noticeable shoulder around 450 ^{o}C in Fig. 12C suggests that Al^{3+} might have accelerated the rate of decomposition (oxidation) implying its influence on reaction kinetics. This observation is in line with early decomposition temperature and early ignition time of PA6/AlMMT sample.

PA6/FeMMT composite, apart from showing strongest 2930 cm^{-1} peak amongst PA6/MI-clay composites, also displayed noticeable peaks within 900-1000 cm^{-1}, 1300-1390/1430-1470 cm^{-1} and 3000-3100 cm^{-1} corresponding to various groups *viz.* =C-H (bend) in trans di-substituted alkenes, aliphatic C-H (rock/bend) and aromatic C-H (stretch)/ unsaturated =C-H (stretch), respectively (pointed out in the inset of Fig. 12D). This indicates that PA6/FeMMT generates higher quantities of unsaturated aliphatic and/or aromatic compounds and also explains its smoke characteristics (Table 1).

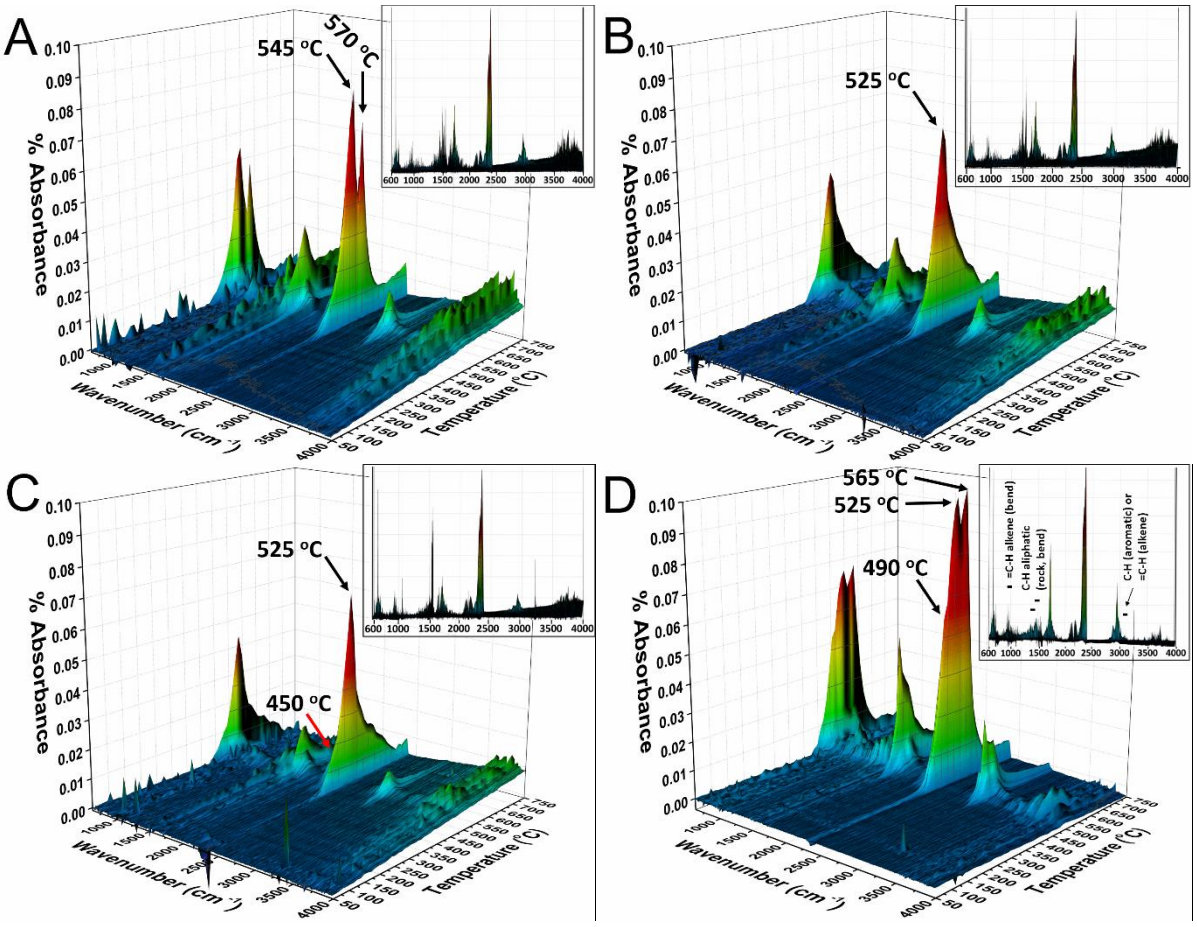

Fig. 12. TG-IR spectra of (A) PA6/NaMMT, (B) PA6/MgMMT, (C) PA6/AlMMT, and (D) PA6/FeMMT. CO_2 (stretch) signals are indicated with arrows. For PA6/NaMMT and PA6/FeMMT composites, peaks at 570 and 565 ^{o}C, respectively, are due to oxidation of

carbonaceous char as seen from Figs. 5 and S6. Presence of only one CO_2 peak in PA6/AlMMT and PA6/MgMMT composites at ~525 ^{o}C indicates that Mg^{2+} and Al^{3+} do not influence oxidation of carbon content in residue beyond 675 ^{o}C. This is also confirmed by FT-IR analysis (Fig. 10A). (Double column fitting image)

3.6 Thermo-oxidative decomposition mechanism

It is anticipated that presence of clay deviates the decomposition path of matrix polymer, but overall decomposition mechanism (in this case, peroxy-based) remains unchanged as it principally depends on polymer backbone structure. Based on the above-discussions, influence of the presence of metal ions (on clay surface) on relevant mechanisms of neat PA6 are given in Figs. 13 and 14. As reported in our previous investigation [26], metal ions have preferential reactivity towards peroxy groups. They can, either oxidize by reducing hydroperoxide group into more reactive peroxy group or reduce by oxidizing hydroperoxide group into another reactive alkoxy group. This indicates that presence of metal ions might help maintain a larger pool of highly reactive peroxy- (I) and/or alkoxy- (II) groups in condensed phase at least during initial stages of decomposition (Fig. 13). According to observations made from condensed phase analysis, plausible pathways for generation of nitrile and isocyanate groups are suggested in Fig. 14. However, concentration of hydroxyl moiety (III) in Fig. 14 is dependent on concentrations of (I) and (II). Hence, role of metal ions in generation of intermediaries (I), (II) and (III) will dictate the early generation of carbo-nitrogenous compounds in condensed phase as seen from Fig. 9.

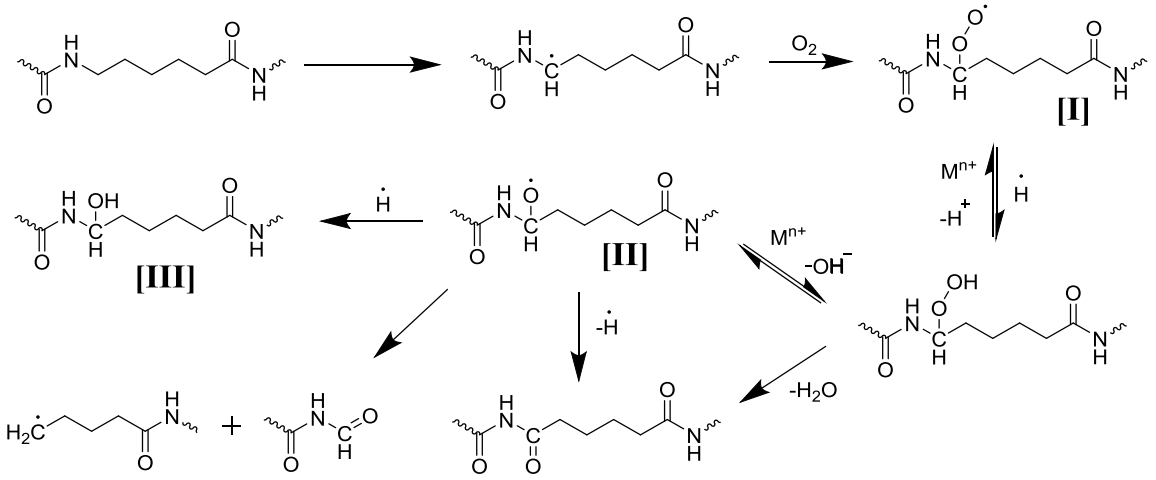

Fig. 13. PA6 decomposition mechanism identified for possible influence of metal ions for accelerated generation of peroxy-/alkoxy- group in condensed phase for PA6/MI-clay nanocomposites. Reversible reactivity of metal ions can maintain the pool of reactive oxy- and peroxy- moieties, creating the environment for possible alternate route of decompositions.

(Double column fitting image)

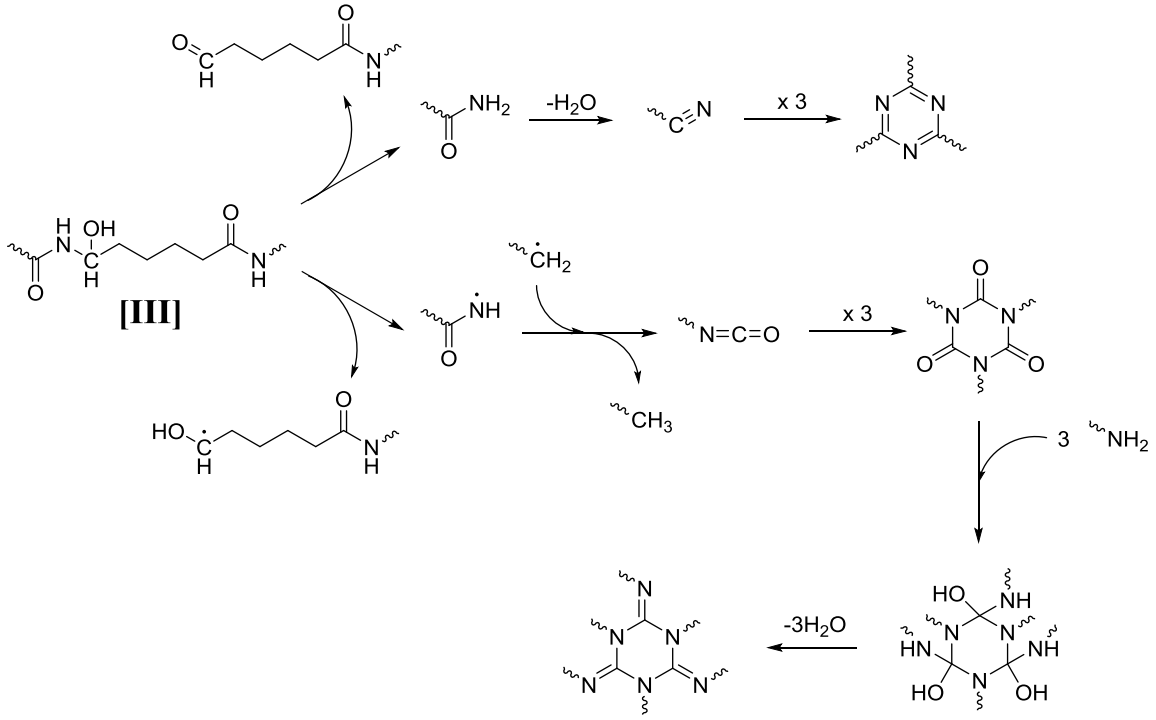

Fig. 14. Possible routes for generation of carbo-nitrogenous residues from intermediate product. The generation and quantity of starting hydroxyl-moiety directly depends on role of metal ions as depicted in Fig. 2. (Double column fitting image)

Based on cone calorimeter results, it is hypothesized that Mg^{2+} and Al^{3+} facilitate preferential formation of oligomeric alkyl radicals at a rate higher than at which they are fragmented and are air-borne resulting in significantly higher quantities of unsaturated compounds. This (along with trapping of volatiles by clay barrier) can facilitate recombination and cross-linking resulting in higher char content as seen from Table 1. It is suggested that depending on their stereo specificity, Mg^{2+}, Al^{3+} and Fe^{3+} will preferentially produce either ordered or amorphous carbonaceous matter as observed from Fig. 10B. However, the oxidative stability of this could not be precisely evaluated in the current work. Further understanding of mechanisms is possible if the evolved gases during cone calorimeter testing are evaluated, which will be the focus of a future work.

Even for PA6/OMI-clay nanocomposites, contour plots are similar (Fig. S6), and differ from neat PA6. This suggests that these materials also follow the decomposition scheme as PA6/MI-clay composites. The much lower quantities of metal ions in OMI-clays and possible shielding of clay platelets resulted in indistinguishable effect between different metal ions. Subsequently, decomposition mechanism becomes independent of cation towards peak decomposition stage and thereon on. Finally, to consolidate the influence of metal ions on PA6 decomposition, curves for selected wavenumbers are shown in Fig. S7 in Supporting Information. These include 2930 cm^{-1} associated with alkane ($–CH_3$, $–CH_2–$), 2358 cm^{-1} (and 680 cm^{-1}) with CO_2 and 1750 cm^{-1}

with C=O. The variations clearly highlight the change in rate of decomposition (decomposition reaction kinetics) as a function of temperature.

4. Conclusions

Current work advances our knowledge of fundamental cause of clay catalysis and the role of different cations on thermo-oxidative stability and combustion properties of PA6/clay nanocomposites. Notably,

1. All exchange metal ions (Mg^{2+}, Al^{3+} and Fe^{3+}) displayed profound effects on decomposition kinetics and mechanisms of PA6/clay composites. Combination of their Lewis acidity and physical barrier (as determined by clay dispersion in the matrix) were important factors.
2. Condensed- and gas-phase analysis provided a qualitative insight into composition of decomposition intermediaries as influenced by clay-polymer interactions (specifically, metal ion-organic interactions).
3. Al^{3+}-rich composites showed accelerated decomposition; Fe^{3+} reduced oxidation stability of char and influenced smoke generation; and Mg^{2+} registered highest char suggesting better thermo-oxidation stability.
4. Primary decomposition reactions prone to be influenced by redox nature of metal ions were identified for PA6.

Acknowledgements

AD acknowledges the Academic Research Fund Tier-1 (RG110/14) from the Singapore's Ministry of Education and National Research Foundation's L2NIC grant (Award No.: L2NICCFP1-2013-4) for financially supporting parts of this research work. Authors are also

grateful to Professors Giovanni Camino and Alberto Frache for their insights and discussions on PA6 decomposition mechanism.

References

[1] J.W. Gilman, T. Kashiwagi, J. Lichtenhan, Nanocomposites: A revolutionary new flame retardant approach, SAMPE J. 33 (1997) 40-46.

[2] A. Dasari, Z-Z. Yu, G-P. Cai, Y-W. Mai, Recent developments in the fire retardancy of polymeric materials, Prog. Polym. Sci. 38 (2013) 1357-1387.

[3] H. Qin, S. Zhang, C. Zhao, G. Hu, M. Yang, Flame retardant mechanism of polymer/clay nanocomposites based on polypropylene, Polymer 46 (2005) 8386-8395.

[4] G. Cai, A. Dasari, Z-Z. Yu, X. Du, S. Dai, Y-W. Mai, J. Wang, Fire response of polyamide 6 with layered and fibrillar nanofillers, Polym. Degrad. Stab. 95 (2010) 845-851.

[5] M.A. Corres, M. Zubitur, M. Cortazar, A. Mugica, Thermal decomposition of phenoxy/clay nanocomposites: Effect of organoclay microstructure, Polym. Degrad. Stab. 98 (2013) 818-828.

[6] T.D. Fornes, P.J. Yoon, D.R. Paul, Polymer matrix degradation and color formation in melt processed nylon 6/clay nanocomposites, Polymer 44 (2003) 7545-7556.

[7] F. Bellucci, G. Camino, A. Frache, A. Sarra, Catalytic charring–volatilization competition in organoclay nanocomposites, Polym. Degrad. Stab. 92 (2007) 425-436.

[8] S.M. Lomakin, I.L. Dubnikova, A.N. Shchegolikhin, G.E. Zaikov, R. Kozlowski, G.M. Kim, G.H. Michler, Thermal degradation and combustion behavior of the polyethylene/clay nanocomposite prepared by melt intercalation, J. Therm. Anal. Calorim. 94 (2008) 719-726.

[9] H. Qin, S. Zhang, C. Zhao, M. Yang, Zero-order kinetics of the thermal degradation of polypropylene/clay nanocomposites, J. Polym. Sci. B Polym. Phys. 43 (2005) 3713-3719.

[10] M.C. Costache, D.D. Jiang, C.A. Wilkie, Thermal degradation of ethylene–vinyl acetate copolymer nanocomposites, Polymer 46 (2005) 6947-6958.

[11] J. Zhu, P. Start, K.A. Mauritz, C.A. Wilkie, Thermal stability and flame retardancy of poly(methyl methacrylate)-clay nanocomposites, Polym. Degrad. Stab. 77 (2002) 253-258.

[12] B.N. Jang, C.A. Wilkie, The effects of clay on the thermal degradation behavior of poly(styrene-co-acrylonitirile), Polymer 46 (2005) 9702-9713.

[13] A. Fina, G. Camino, Ignition mechanisms in polymers and polymer nanocomposites, Polym. Adv. Technol. 22 (2011) 1147-1155.

[14] H.W. Carvalho, C.V. Santilli, V. Briois, S.H. Pulcinelli, Polymer-clay nanocomposites thermal stability: Experimental evidence of the radical trapping effect, RSC Adv. 3 (2013) 22830-22833.

[15] P. Dunn, G.F. Sansom, The stress cracking of polyamides by metal salts. Part II Mechanism of cracking, J. Appl. Polym. Sci. 13 (1969) 1657-1672.

[16] P. Dunn, G.F. Sansom, The stress cracking of polyamides by metal salts. Part I Metal halides, J. Appl. Polym. Sci. 13 (1969) 1641-1655.

[17] S.K. Madan, H.H. Denk, Amides as ligands-II metallic complexes of ϵ-caprolactam, J. Inorg. Nuclear. Chem. 27 (1965) 1049-1058.

[18] L-C. Chao, E-P. Chang, Interaction of anhydrous ferric chloride with nylon 6, J. Appl. Polym. Sci. 26 (1981) 603-610.

[19] B. Lanska, Degradation and stabilization, in: R. Puffr, V. Kubanek (Eds.), Lactam-based polyamides, Vol. I: Polymerization structure and properties, CRC Press, Boca Raton, 1991, pp. 261-302.

[20] G. Sarda, N. Peacock, Action of polar reagents on nylon 66, Nature 200 (1963) 67.

[21] Z. Osawa, Role of metals and metal-deactivators in polymer degradation, Polym. Degrad. Stab. 20 (1988) 203-236.

[22] J. Kriz, J. Dybal, D. Kurkova, P. Arnoldova, I. Prokopova, J. Brozek, Z. Hroch, Molecular structure of the complex of hexano-6-lactam with magnesium bromide, Macromol. Chem. Phys. 202 (2001) 1194-1199.

[23] S.V. Levchik, E.D. Weil, M. Lewin, Thermal decomposition of aliphatic nylons, Polym. Int. 48 (1999) 532-557.

[24] B. Lanska, L. Matisova-Rychla, J. Rychly, Stabilization of polyamides IV. Thermo-oxidation of hexano-6-lactam in the presence of alkali metal salts, Polym. Degrad. Stab. 87 (2005) 361-373.

[25] B. Lanska, L. Matisova-Rychla, J. Rychly, Stabilization of polyamides V. Thermo-oxidation of hexano-6-lactam in the presence of copper salts, Polym. Degrad. Stab. 89 (2005) 534-544.

[26] I.S. Zope, A. Dasari, G. Camino, Elucidating the catalytic effect of metal ions in montmorillonite on thermal degradation of organic modifier, Mater. Chem. Phys. 157 (2015) 69-79.

[27] D.M. Lincoln, R.A. Vaia, R. Krishnamoorti, Isothermal crystallization of nylon-6/montmorillonite nanocomposites, Macromolecules 37 (2004) 4554-4561.

[28] J. Li, Z. Fang, L. Tong, A. Gu, F. Liu, Polymorphism of nylon-6 in multiwalled carbon nanotubes/nylon-6 composites, J. Polym. Sci. B Polym. Phys. 44 (2006) 1499-1512.

[29] A. Fina, H.C.L. Abbenhuis, D. Tabuani, G. Camino, Metal functionalized POSS as fire retardants in polypropylene, Polym. Degrad. Stab. 91 (2006) 2275-2281.

[30] Y. Cai, F. Huang, Q. Wei, L. Song, Y. Hu, Y. Ye, Y. Xu, W. Gao, Structure, morphology, thermal stability and carbonization mechanism studies of electrospun PA6/Fe-OMT nanocomposite fibers, Polym. Degrad. Stab. 93 (2008) 2180-2185.

[31] J. Zhang, Q. Ji, F. Wang, L. Tan, Y. Xia, Effects of divalent metal ions on the flame retardancy and pyrolysis products of alginate fibres, Polym. Degrad. Stab. 97 (2012) 1034-1040.

[32] H.A. Patel, S. Bocchini, A. Frache, G. Camino, Platinum nanoparticle intercalated montmorillonite to enhance the char formation of polyamide 6 nanocomposites, J. Mater. Chem. 20 (2010) 9550-9558.

[33] J. Michal, J. Mitera, J. Kubat, Major pyrolysis and thermoxidative products from certain polyamides, Fire Mater. 5 (1981) 1-5.

[34] D. Fromageot, A. Roger, J. Lemaire, Thermooxidation yellowing of aliphatic polyamides, Die Angew. Makromol. Chem. 170 (1989) 71-85.

[35] J.M. Adams, S. Dyer, K. Martin, W.A. Matear, R.W. McCabe, Diels-Alder reactions catalysed by cation-exchanged clay minerals, J. Chem. Soc. Perkin Transactions 1 6 (1994) 761-765.

[36] A.P. More, A.M. Donald, Mechanical properties of nylon-6 after treatment with metal halides, Polymer 34 (1993) 5093-5098.

[37] T. Sugihara, The influence of some inorganic additives on the formation of the gaseous products from heated nylon 6, Sci. Rep. Fac. Educ. Gifu Univ. Nat. Sci. 6 (1977) 107-114.

Influence of metal ions on thermo-oxidative stability and combustion response of polyamide 6/clay nanocomposites.

Indraneel S Zope[a], Aravind Dasari[a,*], Fanglan Guan[b], Zhong-Zhen Yu[b]

[a]School of Materials Science & Engineering (Blk N4.1), Nanyang Technological University, 50 Nanyang Avenue, Singapore 639798

[b]State Key Laboratory of Organic-Inorganic Composites, College of Materials Science and Engineering, Beijing University of Chemical Technology, Beijing 100029, China

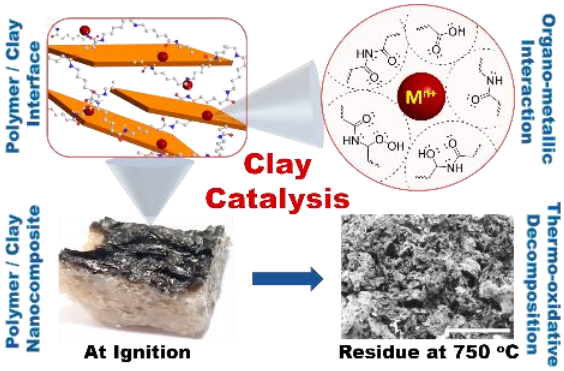

For Table of Contents use only.

Influence of metal ions on thermo-oxidative stability and combustion response of polyamide 6/clay nanocomposites.

Indraneel S Zope[a], Aravind Dasari[a,*], Fanglan Guan[b], Zhong-Zhen Yu[b]

[a]School of Materials Science & Engineering (Blk N4.1), Nanyang Technological University, 50 Nanyang Avenue, Singapore 639798

[b]State Key Laboratory of Organic-Inorganic Composites, College of Materials Science and Engineering, Beijing University of Chemical Technology, Beijing 100029, China

Supplimentary Information

Microstructure

XRD

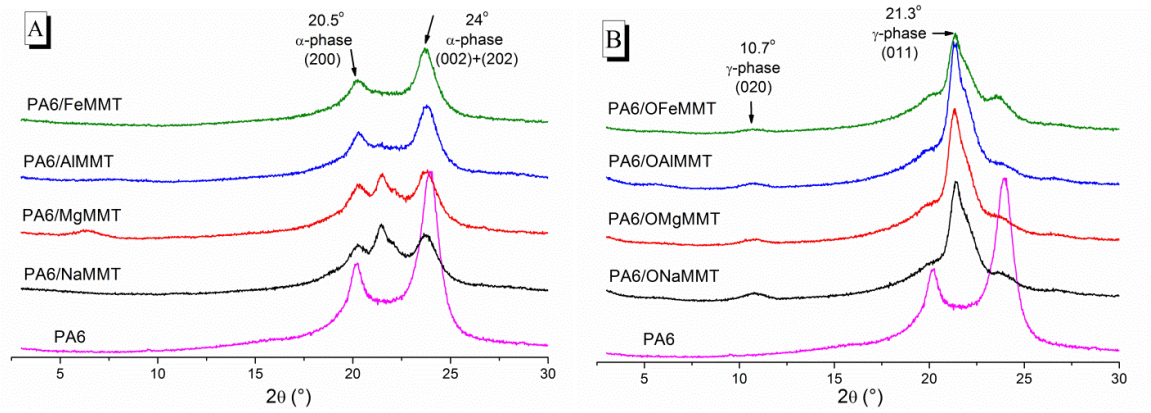

Fig. S1. XRD curves of PA6/MI- and PA6/OMI-clay composites.

DSC

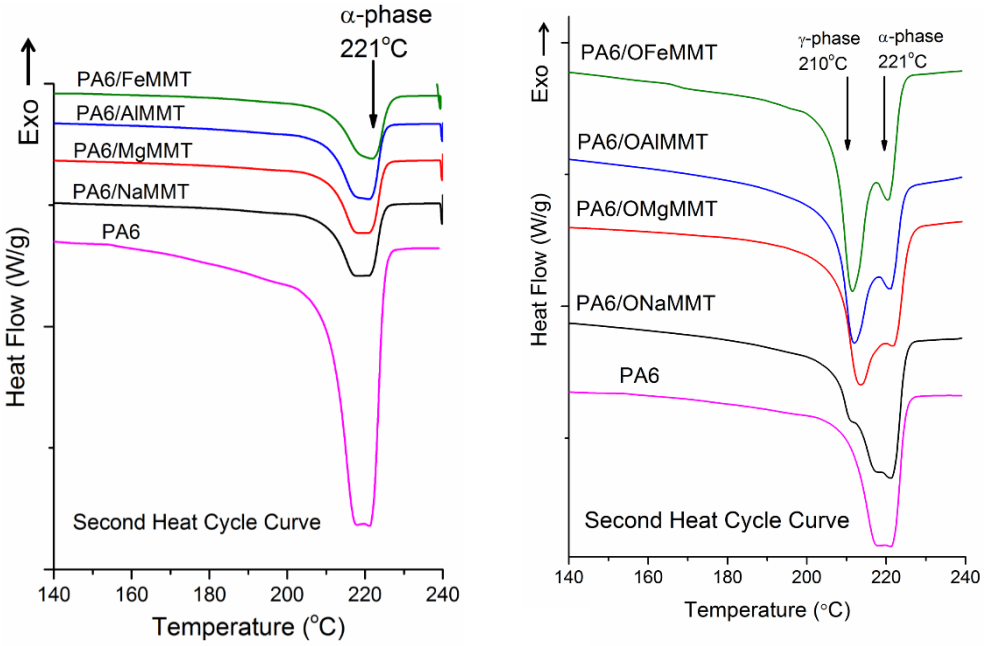

Fig. S2. Second heating cycle curves from DSC for PA6/MI- and PA6/OMI-clay composites.

From DSC thermograms, it is evident that there is no change in melting temperature of PA6/MI-clay composites as compared to neat PA6, suggesting predominance of high melting α

phase. PA6/OMI-clay composites, however, exhibited the presence of both α phase and low melting γ phase, supporting the above XRD results. Ciferri et al. [1] have reported that by the addition of calcium chloride (Ca^{2+} is alkaline earth metal similar to Mg^{2+}) to PA6, melting temperature of PA6 was lowered. Moreover, the % reduction was dependent on metal ion content (see Table S1). In similar studies, it was noted that amide-metal complexation (PA6/Fe^{3+} or PA6/Cr^{3+}) will result in perturbed hydrogen bonding, in turn decreasing crystalline content (Table S1) and higher content of low melting (γ phase) crystallites [2,3].

Table S1. Reported DSC results for PA6/metal halides confirming influence of metal ions on crystallographic properties of PA6.

Reported by	Specimen	Salt Concentration (wt.%)	Melting Point, T_m (^oC)	Melting Enthalpy, ΔH_m (cal/g)	% Crystallinity
Ref [1]	PA6	-	225	16.4	Not reported
	PA6/$CaCl_2$	1	214	13.6	Not reported
		3	212	11.3	Not reported
		5	206	9.0	Not reported
Ref [2]	PA6	-	225	15.2	31.4
	PA6/$FeCl_3$	5	210	12.2	25
		12.5	191	7.6	15.7

It is interesting to see that PA6/OMI-clay nanocomposites show this behavior with successively stronger γ phase peak ($Na^+ < Mg^{2+} < Al^{3+} < Fe^{3+}$) indicating the influence of metal ions on crystallization behavior is in accordance with previously reported studies. Absence of this in PA6/MI-clay composites suggests stearic hindrance experienced by polymer chains in intercalated morphology that limit the complexation during crystallization. Correlating these results with XRD, it can be argued that γ phase development is a function of two different

factors, physical dispersion of clay and nature of interaction between metal ion and neighboring polymer chains. Difference in interactions amongst metal ions with polymer melt might lead to variations in final γ-phase content, however, it will require in-depth study which is currently beyond the scope of this work.

Condensed phase

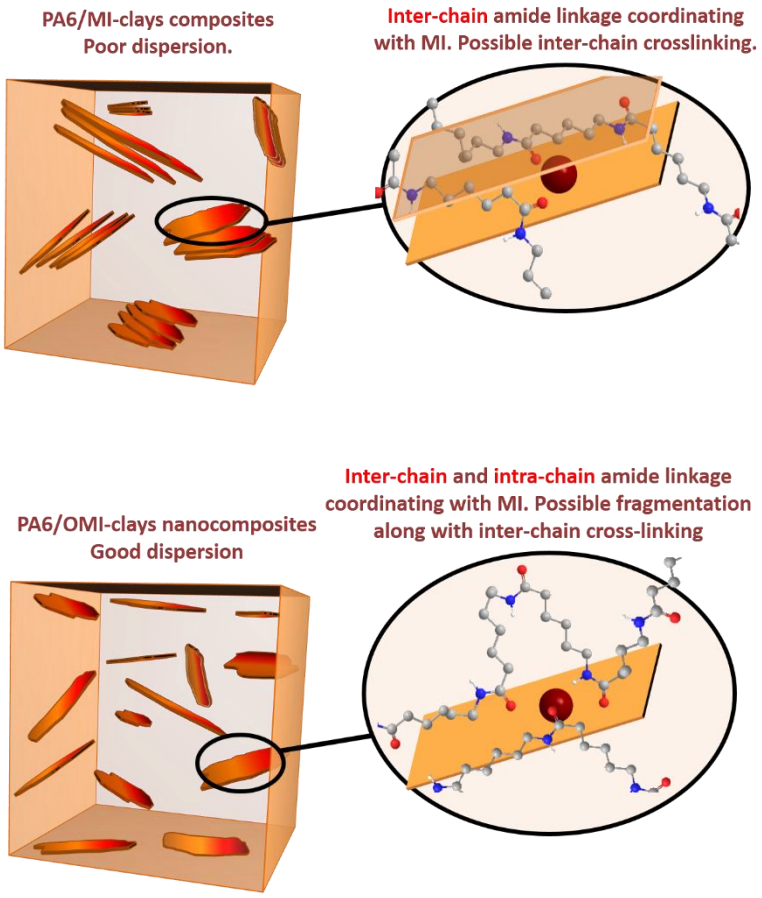

Fig. S3. Schematic of structural collapse of PA6/MI- and PA6/OMI-clay composites. Intercalated systems pose spatial restrictions on polyamide chains confining them within the galleries of platelets. This could influence the formation and conformational stability of coordinate complexes. Possible complexes are reported in Fig. 2 in main manuscript.

Analysis of isothermally heated samples by FT-IR ATR

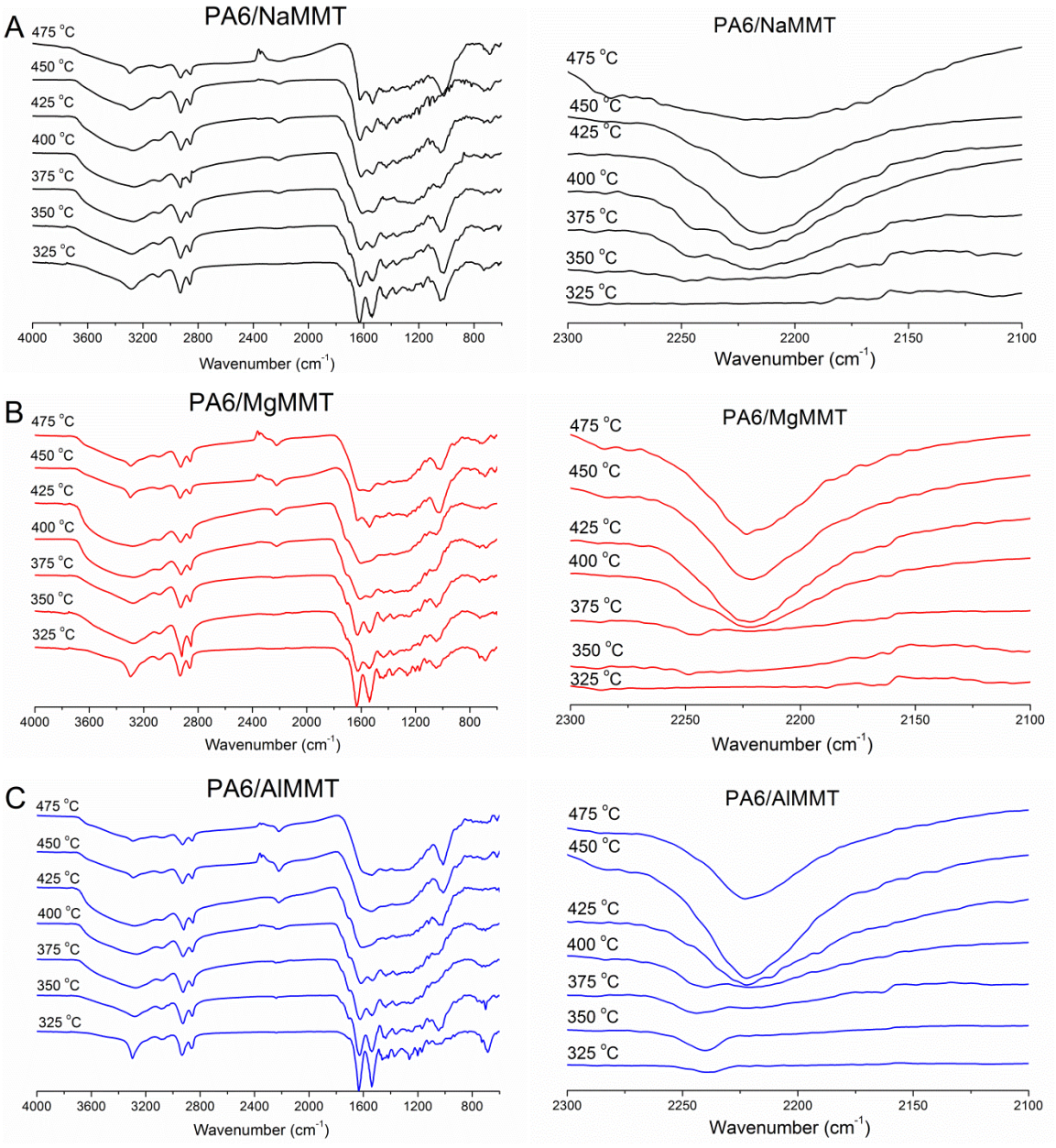

Fig. S4A. Surface FTIR ATR for PA6/MgMMT and PA6/AlMMT nanocomposites.

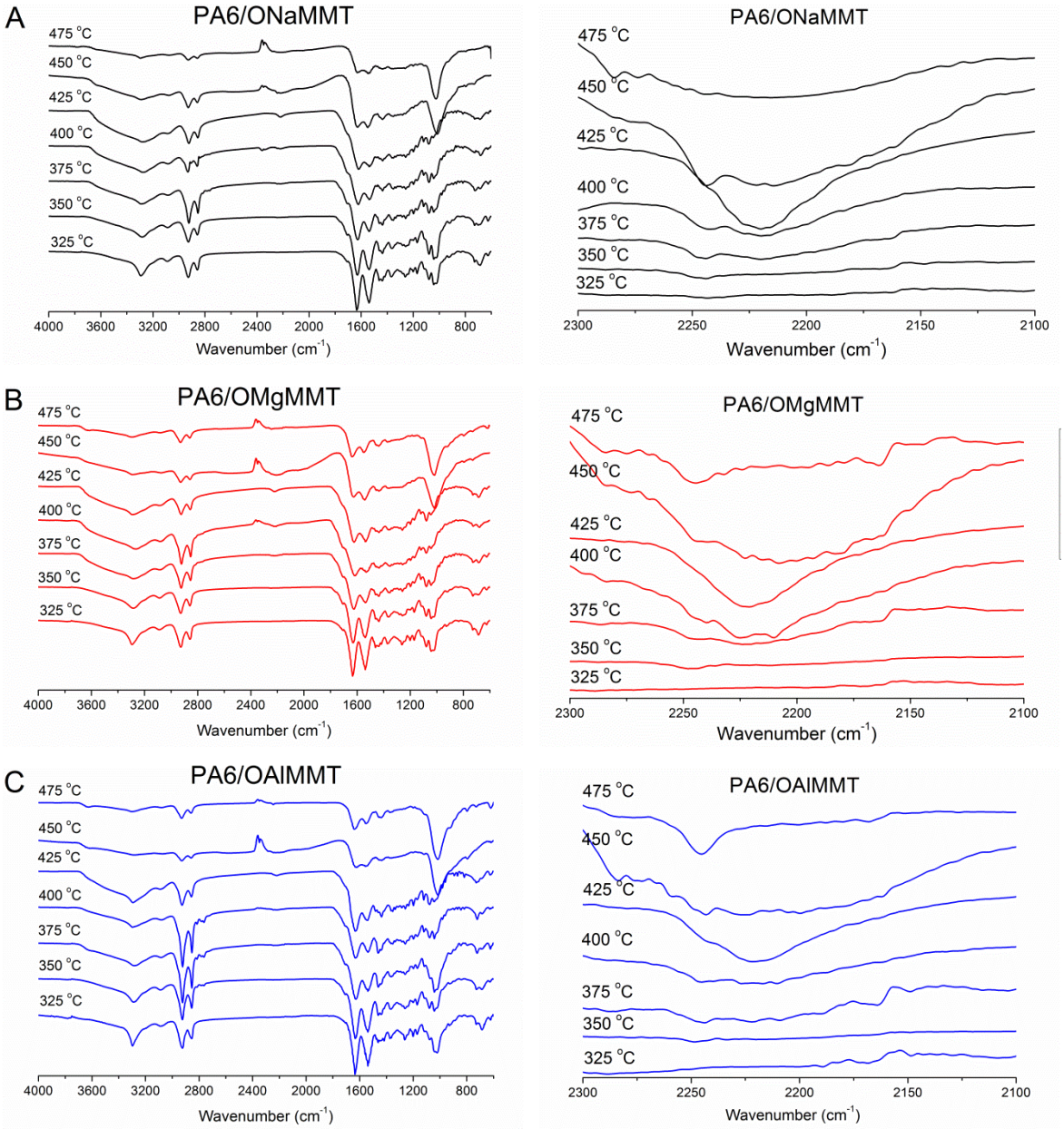

Fig. S4B. Surface FTIR ATR for PA6/OMgMMT and PA6/OAlMMT nanocomposites.

Metal ion migration into Montmorillonite

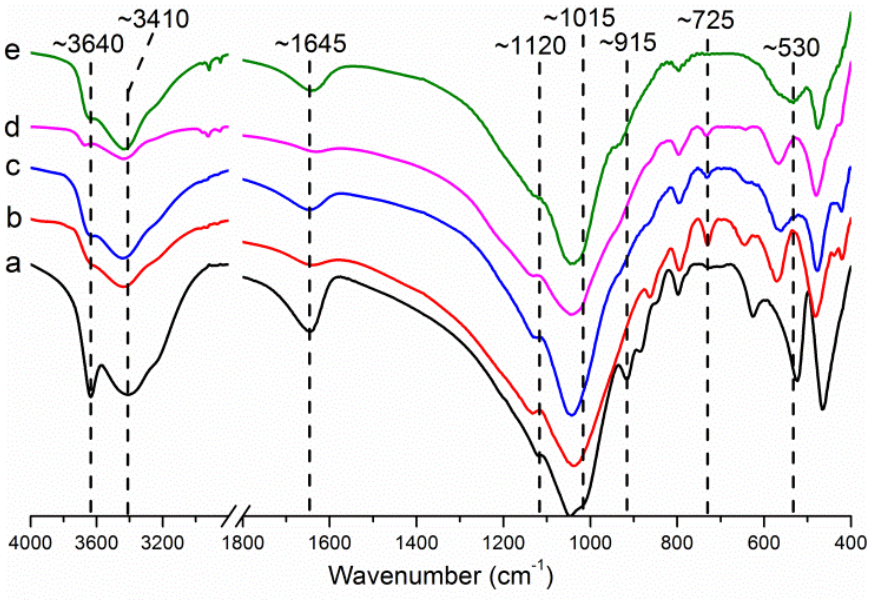

Fig. S5. Powder FT-IR for MgMMT system, (a) dried MgMMT at 110 ^{o}C, (b) MgMMT residue at 750 ^{o}C, (c) OMgMMT residue at 750 ^{o}C, (d) PA6/MgMMT residue at 750 ^{o}C, and (e) PA6/OMgMMT residue at 750 ^{o}C.

It is necessary to understand the fundamental vibrations in montmorillonite (key IR absorption frequencies are reported in Table S2). MgMMT system was chosen as a representative system to provide complete comparison between IR spectra for MgMMT, residues of MgMMT and OMgMMT and residues of PA6/MgMMT and PA6/OMgMMT composites.

R. Tettenhorst [4] reported that upon heating above certain temperatures interlayer cations migrate into the vacant regions of tetrahedral and octahedral layers which subsequently affect the stretching vibration of Si-O_{basal}-Si bond that can be detected using FT-IR. This migration was confirmed by observing shifts in IR bands corresponding to Si-O_{basal} to higher frequencies and decreasing intensity of band corresponding to Al-OH-Al. It is understood that clay sourced from

different parts of world have different composition. As a result, minor differences in original bands positions are expected. However, the shifts in IR bands upon heating are expected to be of similar nature. Accordingly, the shifts observed for band at ~1120 cm^{-1} to higher wavenumber as much as up to ~1135 cm^{-1} for composite residues, possible shift of ~1015 cm^{-1} band to overlap with broad band at 1030 cm^{-1} and diminished band ~915 cm^{-1} can be argued to signify migration of interlayer cation into silica skeleton. Following another reported work by Calvet et al. [5], the shift observed in diminished band from ~915 to ~940 cm^{-1} support the migration of Mg^{2+} into silica skeleton. Migration of cations as big as Cu^{2+} into hexagonal holes upon heating CuMMT up to 350 ^{o}C has also been reported [6]. Bakandritsos et al. [7] reported reduction of intercalated Fe^{3+} to Fe^{2+} and its simultaneous migration to octahedral vacant locations. Although the determination of extend of migration is beyond the scope of this work, it is important to note that size as well as oxidation state of migrated cation can influence its association with structural oxygen. This subsequently could result in strong shoulder at ~1200 cm^{-1}, in the order of Na^{+}< Mg^{2+}< Al^{3+}< Fe^{3+}.

Further, the exact nature of structural bonds corresponding to new band at ~530 cm^{-1} or reason for absence of band at ~725 cm^{-1} in case of PA6/OMgMMT is yet to be identified. However, there are convincing evidences that organic modification of clay induces certain structural modifications in clay otherwise absent at higher temperature. Since these bands are absent in residue for OMgMMT, it appears to occur exclusively in presence of organic polymer matrix.

Table S2. FT-IR for MMT

Typical absorption frequencies, cm^{-1}	**Assignments**
~3640	OH-stretching
~3400	OH-stretching
~1645	OH-bending
~1120, ~1045 and ~1015	Si-Obasal-Si
~1080	Si-Oapical-Si
~915	Al-OH-Al
~880	Al-OH-Fe
~840	Al-OH-Mg
~525	Si-O-Al (bend)
~470	Si-O-Si (bend)

Lastly, it is important to apprehend the influence of structural composition of clay on migration of interlayer cations. Purnell et al. [8] observed that for montmorillonite originated from Texas, cations like Ni^{2+}, Co^{2+} and Zn^{2+} displayed migration phenomena upon heating respective cation exchanged clays. This was reported to be in complete contrast to bentonite clay originated from Wyoming region. This is a very crucial observation and potentially highlights the possible influence of inherent clay chemistry upon polymer matrix decomposition.

Gas phase analysis using thermogravimetric coupled Fourier transform infrared spectroscopy

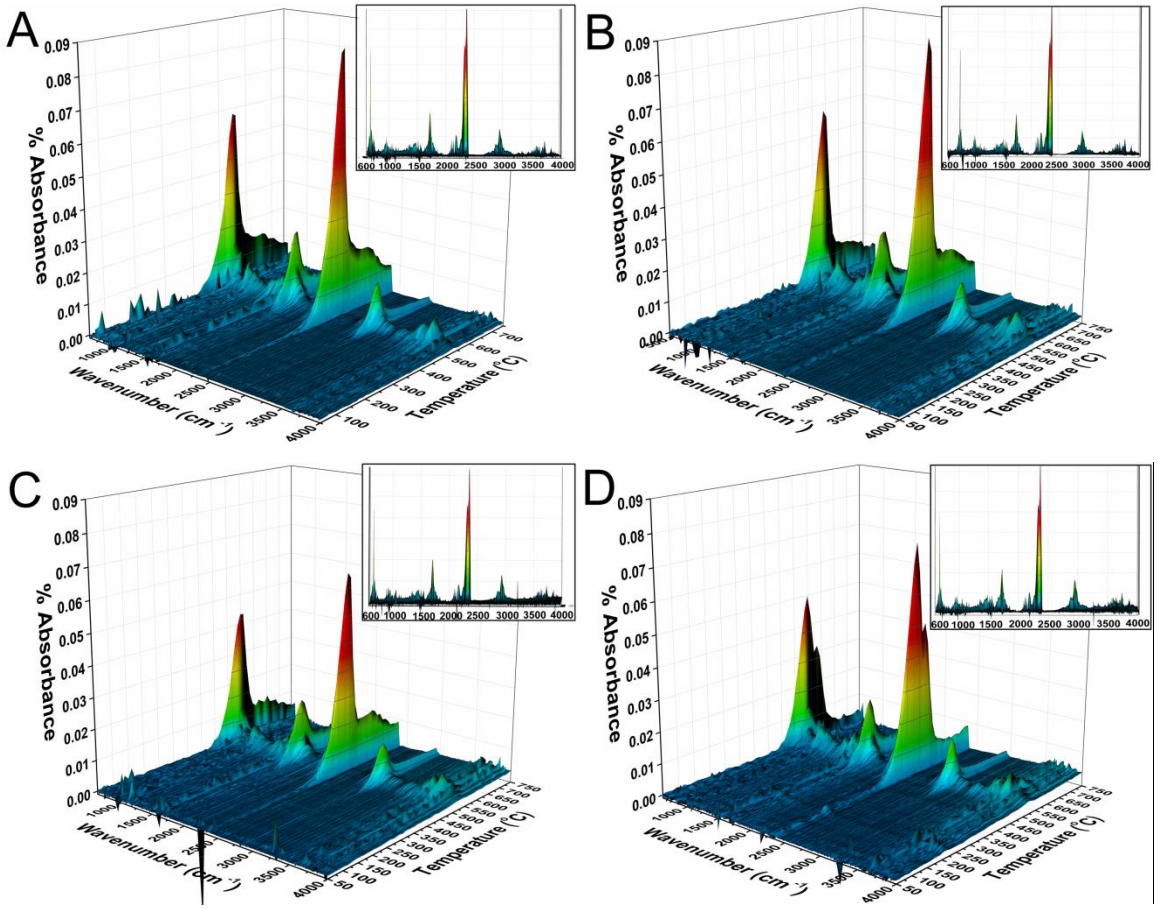

Fig. S6. TG-IR spectra, PA6/ONaMMT (A), PA6/OMgMMT (B), PA6/OAlMMT (C), PA6/OFeMMT (D).

Except for twin peak in CO_2 evolution profile for PA6/OFeMMT, rest all composites showed very similar single peak, no other observable difference was noted apart from peak CO_2 evolution temperatures. Supporting the theory proposed earlier suggesting restricted interaction

of interlayer cations with neighboring decomposing PA6 chains, as a result of shielding effect on metal ions. This may result into similar decomposition pattern for all PA6/OMI-clays giving similar TG-IR contour plots. PA6/OFeMMT continue to show second peak at 565 ^{o}C, although with much lower intensity, thus, it may be argued that catalytic activity of Fe^{3+} was subdued due to surface coat. Lower concentration and comparatively lower catalytic activity of Na^{+} as compared to Fe^{3+} may possibly explain the disappearance of second peak in CO_2 emission profile otherwise observed at 570 ^{o}C in case of PA6/NaMMT.

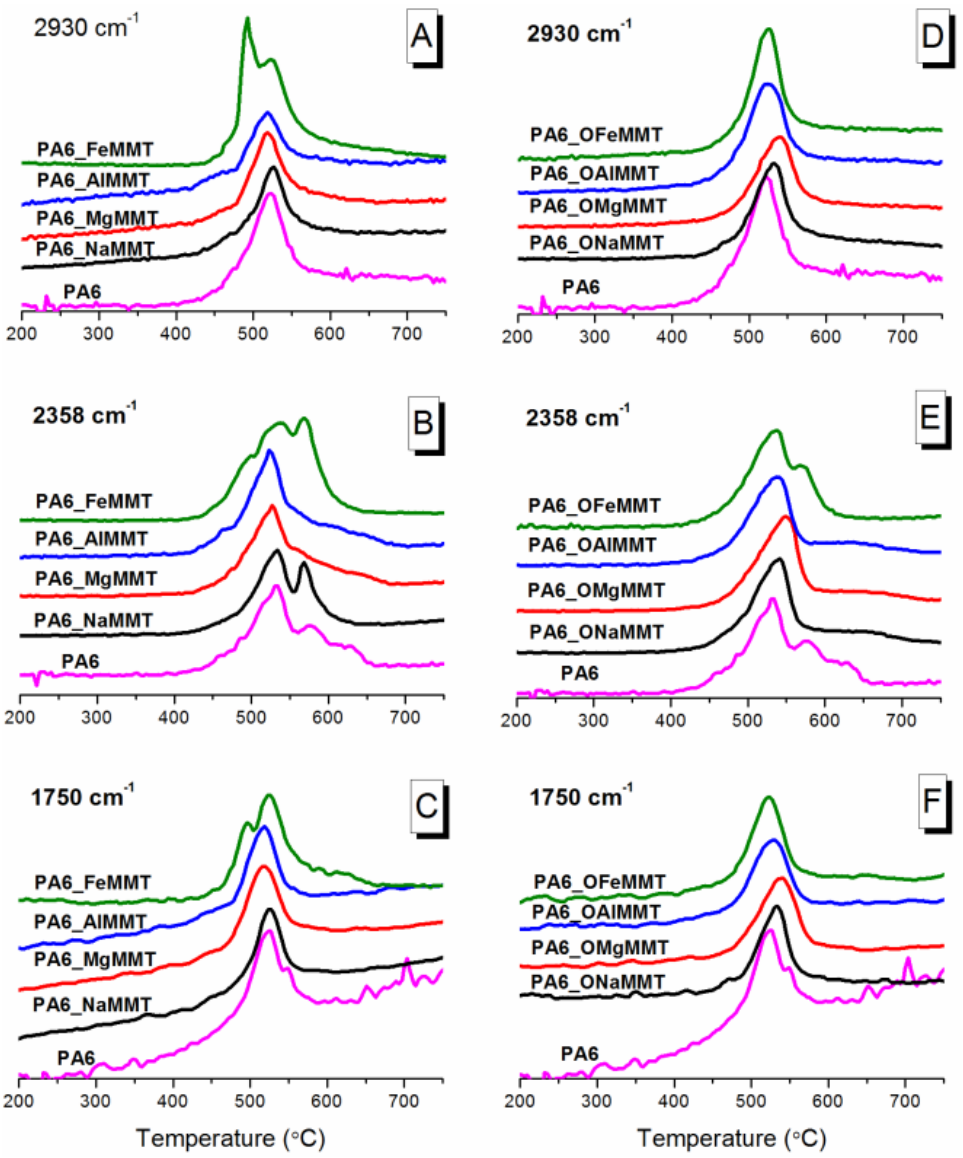

Fig. S7. IR spectra for 2950, 2358 and 1750 cm^{-1}.

There are two important observations for PA6/FeMMT that can be associated with its decomposition mechanism. From Fig. S7, (1) a very sharp maxima for 2930 cm^{-1} curve and (2) distinct maxima in 1750 cm^{-1} curve around 480 ^{o}C overlapping with onset of oxidation as seen from shoulder in 2358 cm^{-1} curve, indicates early generation of aliphatic C-H and C=O containing compounds. The evident shift in peak temperatures indicate the influence of metal ions on generation of different compounds, conservatively associated to decomposition kinetics.

References

[1] A. Ciferri, E. Bianchi, F. Marchese, A. Tealdi, Differential scanning calorimetry of poly(caproamide)/inorganic salt systems, Die Makromol. Chem. 150 (1971) 265-270.

[2] L.-C. Chao, E.-P. Chang, Interaction of anhydrous ferric chloride with nylon 6, J. Appl. Polym. Sci. 26 (1981) 603-610.

[3] A. Szafner, J. Karger-Kocsis, Increase of the melt viscosity of polycaproamide by chromium (III) ions, Polymer 16 (1975) 879-880.

[4] R. Tettenhorst, Cation migration in montmorillonites, The American Mineralogist 47 (1962) 769-773.

[5] R. Calvet, R. Prost, Cation migration into empty octahedral sites and surface properties of clays, Clay Clay. Miner. 19 (1971) 175-186.

[6] L. Heller-Kallai, C. Mosser, Migration of Cu ions in Cu montmorillonite heated with and without alkali halides, Clay Clay. Miner. 43 (1995) 738-743.

[7] A. Bakandritsos, A. Simopoulos, D. Petridis, Iron changes in natural and Fe(III) loaded montmorillonite during carbon nanotube growth, Nanotechnol. 17 (2006) 1112.

[8] J. Purnell, L. Yun, Ionic migration and charge reduction in Ni^{2+}, Co^{2+} and Zn^{2+}-exchanged Texas montmorillonite, Catal. Lett. 18 (1993) 235-241.